



ELSEVIER

Available online at www.sciencedirect.com

SCIENCE @ DIRECT®

JOURNAL OF
**CRYSTAL
GROWTH**

Journal of Crystal Growth 259 (2003) 273–278

www.elsevier.com/locate/jcrysgro

New methods for fabricating patterned lithium niobate for photonic applications

V. Joshkin^{a,b,c}, K. Dovidenko^d, S. Oktyabrsky^d, D. Saulys^{a,e},
T. Kuech^f, L. McCaughan^{a,g,*}

^a *Materials Research Science and Engineering Center, University of Wisconsin-Madison, 1415 Engineering Dr., Madison, WI 53706, USA*

^b *Department of Materials Science and Engineering, University of Wisconsin-Madison, Madison, WI, USA*

^c *Focused Research, Inc., 8551 Reaserch Way, Middleton, WI 53562, USA*

^d *School of Nanosciences and Engineering, University of Albany Institute for Materials, 251 Fuller Road, Albany, NY 12203, USA*

^e *Department of Chemistry, University of Wisconsin-Madison, Madison, WI, USA*

^f *Department of Chemical Engineering, University of Wisconsin-Madison, Madison, WI, USA*

^g *Department of Electrical and Computer Engineering, University of Wisconsin-Madison, 1415 Engineering Dr., Madison, WI 53706, USA*

Received 27 June 2003; accepted 4 August 2003

Communicated by R.S. Feigelson

Abstract

The inherently large chemical stability of crystalline LiNbO₃ has effectively precluded the use of standard photolithographic patterning techniques. We present a two-stage growth method for fabricating patterned crystalline LiNbO₃ structures for photonic applications. The method uses atmospheric chemical vapor deposition (CVD) to produce an amorphous LiNbO₃ film. The film can be patterned using conventional photolithography and rapidly etched (> 5 μm/min) with wet or dry chemical techniques. Alternatively, a standard lift-off process, using SiO₂ as a masking material, can be used to produce a desired pattern. When grown on LiNbO₃ substrates, a post-growth anneal converts the amorphous film to single-crystal LiNbO₃.

© 2003 Elsevier B.V. All rights reserved.

Keywords: A3. Chemical vapor deposition; B1. Oxides; B2. Nonlinear optical materials

1. Introduction

The large second-order ($\chi^{(2)}$) nonlinearities of LiNbO₃, have made it possible to demonstrate an impressive array of electro-optic and all-optical wave-mixing processes. These include traveling

wave modulators [1,2], optical switch arrays [3], wavelength converters [4,5], and tunable mid-IR coherent light sources [6]. The large refractive index of LiNbO₃ ($n \sim 2.2$) also makes it an attractive material for 2D linear photonic crystals [7]. Practical LiNbO₃ device fabrication is thus far based on limited processing techniques applied to bulk material. The absence of a viable thin film growth technique and the inherent chemical inertness of the material severely limit this technology. As an example, optical ridge

*Corresponding author. Tel.: +1-608-2620311; fax: +1-608-2654623.

E-mail address: mccaughan@enr.wisc.edu
(L. McCaughan).

waveguides have been proposed as a method to significantly lower the operating voltage of LiNbO₃ traveling wave modulators. Direct etching (e.g., by RIE) of a LiNbO₃ wafer, however, produces optically rough features with large optical losses [8].

We describe two new related methods for producing high aspect ratio topographic features in LiNbO₃ [9]. These methods are based on the physical and chemical properties of amorphous LiNbO₃ films grown by atmospheric pressure chemical vapor deposition (CVD) from alkoxide precursors. Unlike crystalline LiNbO₃, the amorphous films are easily etched. When grown on a LiNbO₃ substrate and properly annealed, the patterned amorphous material becomes single crystal. Shaping of the thin films can be effected by either standard wet or dry chemical etching or a lift-off process.

2. Experimental procedure

Fig. 1 shows a schematic view of the atmospheric pressure CVD system used to grow amorphous LiNbO₃ films. Substrates (~1 cm², c-cut LiNbO₃) were loaded into the horizontal reactor, which was heated by a furnace. Before growth the substrates were annealed at 1100°C for 1 h. Films were deposited from lithium t-butoxide and niobium ethoxide (maintained at 190°C and 150°C, respectively). The delivery gas line was kept at 150°C to prevent deposition inside the line.

A carrier gas of 23% oxygen and 77% nitrogen was bubbled through the precursors at a flow rate ~0.5 slpm. Film growth rate and film crystallinity are highly dependent on reactor temperature. Under the conditions employed here, a growth rate of ~2 μm/h was observed at reactor temperatures between ~500°C and 750°C. Growth of amorphous films was typically carried out at a substrate temperature of ~650°C. Films grown over the temperature range of 500–700°C were amorphous, however, higher growth temperatures, >700°C yielded polycrystalline or crystalline films. The chemical composition of the amorphous LiNbO₃ films was examined with Auger electron spectroscopy using films grown on (111) Si to obviate surface charging. As seen in Fig. 2, no elemental carbon was detected in a typical film. The amorphous films were crystallized by annealing them in a closed ceramic container containing powdered LiNbO₃. To further insure an adequate lithium oxide pressure over the films, the samples were also covered with a bulk LiNbO₃ wafer segment. Annealing was performed for one hour at 900–1100°C.

Grown films were analyzed by optical (Nomarski differential interference contrast), secondary electron, and high-resolution electron microscopies. X-ray diffraction (XRD) scans (Cu Kα source, incident beam 74° to film surface normal) were recorded with a two-dimensional X-ray detector. In-plane grain alignment was examined using XRD pole figure φ-scans around the film plane normal. (Figs. 3a and b). These were

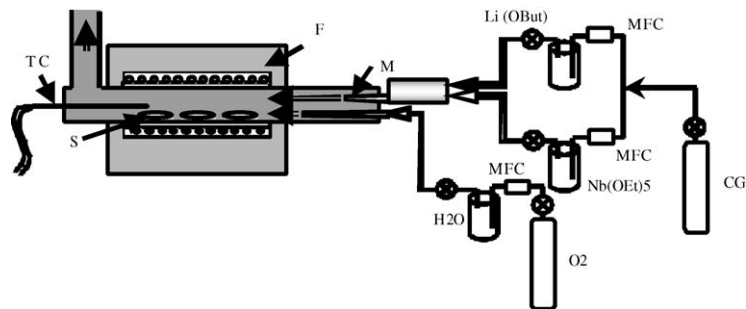


Fig. 1. Schematic representation of the atmospheric pressure CVD system for lithium niobate growth: TC—thermocouple, S—substrates, F—furnace, M—mixing zone of gas inlet system; MFC—mass flow controllers. Precursor bubblers are indicated by Li(OBut) and Nb(OEt)₅, respectively; and CG indicates the carrier gas. A supplemental wet oxygen supply line is shown but was not used in these experiments. Crossed circles show manual valves.

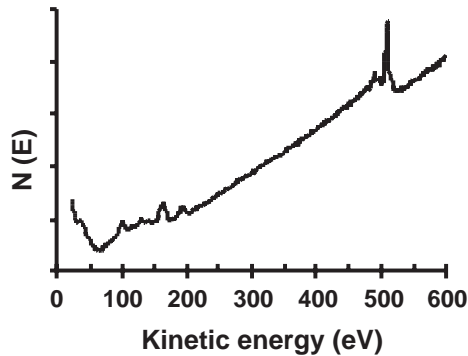


Fig. 2. Auger electron spectra of amorphous LiNbO_3 films grown by CVD on a $\text{Si}(111)$ substrate. The peaks are due to the following elements (orbital transitions in parentheses): (a) ~ 45 eV, Li(KLL); (b) ~ 100 eV, Si(LMM); (c) ~ 160 eV, Nb(MNN); (d) ~ 280 eV, C(KLL)-absent; and (e) ~ 500 eV O(KLL).

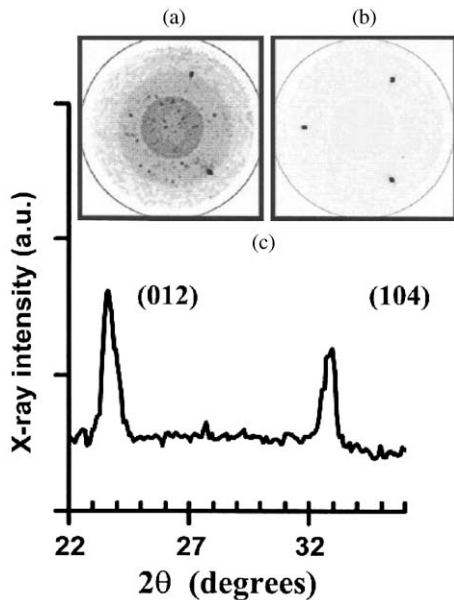


Fig. 3. X-ray diffraction data of a LiNbO_3 film grown on a c-cut LiNbO_3 substrate. (a) (012) pole plot taken of an as-grown amorphous film (growth temperature $\sim 650^\circ\text{C}$); diffuse scattering dominates the weak substrate diffraction spots. (b) (012) pole plot of the amorphous film after a 1-h anneal at 1100°C ; no diffuse scattering; single set of diffraction spots. (c) X-ray diffraction scan of the annealed film.

constructed for the (104) diffraction peak ($\theta = 16^\circ$) by overlaying the ϕ -scans around the film plane normal on a polar plot. On these plots

in-plane misorientation is seen as azimuthal arcs. The degree of out of plane alignment was measured using the integrated intensity of the pole figure plotted as a function of θ (Fig. 3c). Dry etching was performed with the RIE system Plasma-Therm 1440. A standard photoresist (PR1827) was used in both dry and wet etching experiments. Thickness measurements on patterned films were performed with a profilimeter.

3. Results and discussion

High growth rates or lower growth temperatures generate amorphous, as opposed to polycrystalline or epitaxial, LiNbO_3 films. Films grown between $\sim 500^\circ\text{C}$ and 650°C were amorphous, as evidenced by a diffuse X-ray diffraction band overlaying weak diffraction peaks from the substrate (Fig. 3a). After a one hour post-growth anneal at 1100°C , X-ray diffraction scans using a 2-D X-ray detector and pole plots derived from them show the previously amorphous film grown at 650°C to be single crystal (Fig. 3b). The degree of out-of-plane misorientation can be estimated from a plot of the integrated diffraction intensity at constant θ (taken from the pole plot) vs. diffraction angle, 2θ (Fig. 3c). Here, diffraction peak widths are of the order of the instrument resolution ($\Delta 2\theta \sim 0.5^\circ$).

The single-crystal epitaxial nature of the annealed LiNbO_3 layer was confirmed by transmission electron microscopy (TEM) from $\sim 1 \mu\text{m}$ films (Fig. 4). The cross-sectional TEM image of the LiNbO_3 layer after annealing taken under $[\bar{2}110]$ two-beam bright field conditions is consistent with single-crystal structure. The inclined lines are bend contours, the appearance of which means that the material is single crystal. That these lines propagate continuously below the $\sim 1 \mu\text{m}$ film indicates that the film is not a second phase. The light/dark boundary is a thickness fringe—a point at which the thickness of the sample in the direction of the electron beam changes. Its position can be moved by changing imaging conditions. No interface between the film and the substrate, or associated defects, was visible under different sets of two-beam imaging conditions, consistent with a

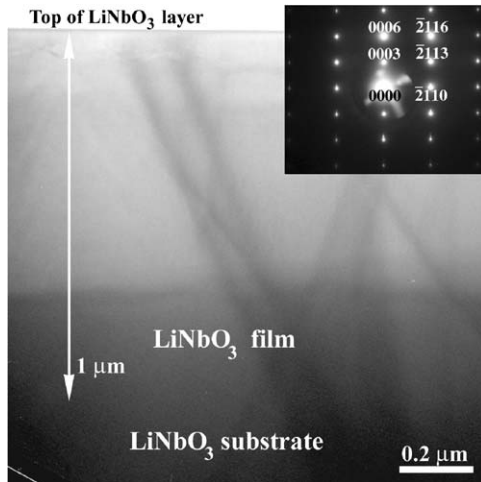


Fig. 4. Cross-sectional TEM image of an amorphous LiNbO_3 film after annealing for 1 h at 1100°C . The image is taken under $[\bar{2}110]$ two-beam bright field conditions with the electron beam close to the $[01\bar{1}0]$ direction of LiNbO_3 . The inset is the corresponding $[01\bar{1}0]$ zone axis SADP taken from the film/substrate interface area in the image, demonstrating the single-crystal epitaxial nature of the layer. The inclined lines are bend contours; the horizontal band is a thickness fringe.

high quality crystalline film and intermixing at the interface. Films typically had a dislocation density of less than 10^6 cm^{-2} .

Analysis of selected area diffraction patterns (SADPs), obtained from different areas consisting only of the film, as well as from areas containing both the film and substrate, confirmed that LiNbO_3 film is epitaxial single crystal. A typical SADP (inset Fig. 4) taken from an area ($1.5\mu\text{m}$ dia.) containing both the film and the substrate consists of one set of spots and corresponds to the $[01\bar{1}0]$ zone of the rhombohedral LiNbO_3 crystal structure with $a = 0.515\text{ nm}$, $c = 1.386\text{ nm}$, space group $R3c$ (161). This SADP demonstrates that there is no difference in crystal structure, orientation or crystal quality between the LiNbO_3 film and substrate. The TEM analysis proves the high-quality crystallized LiNbO_3 layer to be free of segregations of a second phase and extended defects. Films grown at higher temperatures ($\sim 700\text{--}750^\circ\text{C}$) exhibited diffraction rings in the X-ray diffraction pole plots characteristic of polycrystalline films (not shown).

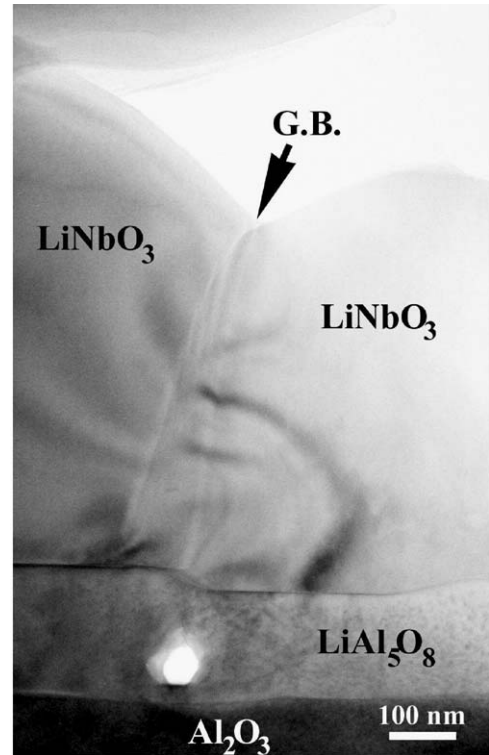


Fig. 5. TEM cross-section image of LiNbO_3 film grown on $[0001]$ Al_2O_3 . The film was grown at 700°C and annealed for 1 h at 1100°C .

For comparison, we deposited and annealed LiNbO_3 ($a = 0.515\text{ nm}$) films as above on $[0001]$ Al_2O_3 ($a = 0.476\text{ nm}$). While films grown and annealed on LiNbO_3 were always epitaxial (Figs. 3 and 4), LiNbO_3 films on sapphire were always polycrystalline with an average grain size of about $1\mu\text{m}$. As can be seen in the cross-sectional TEM (Fig. 5), an interfacial layer $\sim 200\text{ nm}$ thick forms between the Al_2O_3 substrate and the LiNbO_3 film. X-ray diffraction shows this interlayer to be LiAl_5O_8 —likely due to a diffusion of highly mobile Li^+ to the $\text{LiNbO}_3\text{--Al}_2\text{O}_3$ interface, forming a reaction couple. A sufficiently high Li_2O activity during growth or anneal would allow the thermodynamically favored formation of additional phases. As seen in a cross-section TEM of the interface (Fig. 6), the LiAl_5O_8 (cubic structure with $a = 0.791\text{ nm}$) layer is epitaxial with the sapphire substrate, with the (111) direction of



Fig. 6. High-resolution TEM cross-section image of the $\text{LiAl}_5\text{O}_8/\text{Al}_2\text{O}_3$ interface. The film was grown on $[0001]$ Al_2O_3 at 700°C and annealed for 1 h at 1100°C .

LiAl_5O_8 parallel to the (0001) of sapphire. However, any initial epitaxial relationship between the LiNbO_3 and either the LiAl_5O_8 or Al_2O_3 is lost by the time the reaction is complete. (LiAl_5O_8 has about an 8% lattice mismatch with LiNbO_3 .) Also present are small (~ 100 nm) second phase inclusions in the LiNbO_3 layer. Energy dispersive X-ray analysis shows the presence of excess oxygen in these inclusions as compared to the bulk of the LiNbO_3 film, indicating the presence of perhaps of Nb_2O_5 or a different Li–Nb–O phase. TEM revealed no second phase inclusions associated with the LiNbO_3 grain boundaries or at the $\text{LiNbO}_3/\text{LiAl}_5\text{O}_8$ interface.

Advantage can be taken of the rapid etch rate of amorphous LiNbO_3 ($\sim 7\ \mu\text{m}/\text{min}$ in 4% HF at room temperature) to pattern the film before annealing to crystallinity. Fig. 7a is an electron micrograph of a photolithographically patterned, HF:H₂O etched and then annealed LiNbO_3 film. A non-optimized RIE etch using a 29:2::CF₄:O₂ gas mixture and 50 W RF power etched the amorphous LiNbO_3 ~ 20 -fold faster than for crystalline or polycrystalline LiNbO_3 under the same conditions. The variation in the size of the rhombohedral features is a result of undercutting due to imperfect masking of the small ($\sim 1\ \text{cm}^2$) substrates. Nevertheless, the presence of $\sim 1\ \mu\text{m}^3$ features indicates that the bulk film diffusion processes which occur at annealing temperatures during crystallization are more effective than the surface mobility in altering the structure of the resulting film.

A lift-off technique was also used to shape lithium niobate thin films. A photolithographically

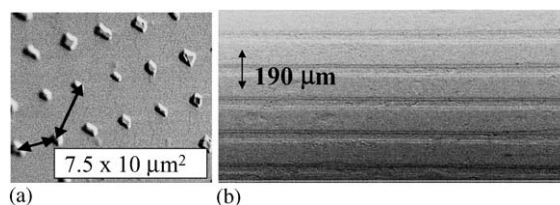


Fig. 7. Images of patterned films: (a) scanning electron micrograph of a photolithographically patterned, etched in 4% HF, and annealed (1000°C) LiNbO_3 film; (b) optical micrograph of a set of $140\ \mu\text{m}$ ridges on a $190\ \mu\text{m}$ periodicity, formed by SiO_2 masking and lift-off.

patterned SiO_2 mask atop a crystalline lithium niobate substrate was overgrown with LiNbO_3 , at a temperature ($\sim 800^\circ\text{C}$) consistent with polycrystalline formation. The LiNbO_3 -overgrown SiO_2 regions etched easily in an aqueous HF solution, likely a result of a reaction between the SiO_2 mask and LiNbO_3 film, while the LiNbO_3 deposited directly on the LiNbO_3 substrate was unaffected. After annealing, the resulting $1\ \mu\text{m}$ thick by $100\ \mu\text{m}$ wide patterned film (Fig. 7b) was single crystal, as determined by X-ray diffraction (not shown). Lift-off processes are not often successfully applied to perovskite films: the higher temperatures necessary for epitaxial perovskite growth typically can induce a reaction or interdiffusion of the oxide and the mask material. Thus, this procedure may prove to be of general utility with regard to the shaping of otherwise intractable metal oxide thin films (e.g., ridge waveguides).

In summary, we present two related new methods for producing deep patterned features in mono-crystalline LiNbO_3 . Atmospheric CVD is used to deposit LiNbO_3 at a sufficiently large deposition rate that an amorphous film is produced. This film is easily patterned using chemical or lift-off techniques, and can subsequently be crystallized without serious distortions of the feature.

Acknowledgements

This work is supported by the Materials Research Science and Engineering Center at the

University of Wisconsin-Madison, and grants from the Electronics, Photonics and Device Technologies Program of the ECS Division of the NSF, from the AFOSR, and the ONR.

References

- [1] E.L. Wooten, K.M. Kissa, A. Yi-Yan, E.J. Murphy, D.A. Lafaw, P.F. Hallemeier, D. Maack, D.V. Attanasio, D.J. Fritz, G.J. McBrien, D.E. Bossi, *IEEE J. Selected Topics Quantum Electron.* 6 (2000) 69.
- [2] F. Heismann, S.K. Korotky, J.J. Veselka, Lithium niobate integrated optics: selected contemporary devices and system applications, in: B.I.P. Kaminow, T.L. Koch (Eds.), *Optical Fiber Telecommunications III*, Academic Press, San Diego, 1997, pp. 377–462.
- [3] E.J. Murphy, T.O. Murphy, A. Ambrose, R. Irvin, B. Lee, P. Peng, G. Richards, A. Yorinks, *J. Lightwave Technol.* 14 (1996) 352.
- [4] M.H. Chou, I. Brener, M.M. Fejer, E.E. Chaban, S.B. Christman, *IEEE Photon. Technol. Lett.* 11 (1999) 653.
- [5] A. Chowdhury, S.C. Hagness, L. McCaughan, *Opt. Lett.* 25 (2000) 832.
- [6] G.Y. Wang, J. Zhao, Q. Chen, M. Cronin-Golomb, *Appl. Phys. Lett.* 70 (1997) 2218.
- [7] C. Manolatu, S. Johnson, S. Fan, P. Villeneuve, H. Haus, J. Joannopoulos, *J. Lightwave Technol.* 17 (1999) 1682.
- [8] J.L. Jackel, R.E. Howard, E.L. Hu, S.P. Lyman, *Appl. Phys. Lett.* 38 (1981) 907.
- [9] US Patent No. 6,545,791, Electro-Optic Optical Elements.